Acta Crystallographica Section D
Biological Crystallography
ISSN 0907-4449

Structural evidence for the inhibition of grape dihydroflavonol 4-reductase by flavonols

Nadia Trabelsi,[a,b] Pierre Petit,[a,c] Claude Manigand,[a] Béatrice Langlois d'Estaintot,[a] Thierry Granier,[a] Jean Chaudière[a] and Bernard Gallois[a]*

[a]CBMN, UMR CNRS 5248, Bâtiment B8, Avenue des Facultés, Université Bordeaux 1, 33405 Talence CEDEX, France, [b]Centre de Biotechnologie de Borj-Cedria, BP 901, 2050 Hamman-Lif, Tunisia, and [c]BioXtal, c/o AFMB, UMR 6098 CNRS–Universités Aix-Marseille I et II, Campus de Lumigny, Case 932, 163 Avenue de Lumigny, 13288 Marseille CEDEX 09, France

Correspondence e-mail: b.gallois@cbmn.u-bordeaux.fr

Received 10 April 2008
Accepted 11 June 2008

PDB References: grape dihydroflavonol 4-reductase, 3bxx, r3bxxsf; 3c1t, r3c1tsf.

Dihydroflavonol 4-reductase (DFR) is a key enzyme of the flavonoid biosynthesis pathway which catalyses the NADPH-dependent reduction of 2*R*,3*R*-*trans*-dihydroflavonols to leucoanthocyanidins. The latter are the precursors of anthocyans and condensed tannins, two major classes of phenolic compounds that strongly influence the organoleptic properties of wine. DFR has been investigated in many plant species, but little was known about its structural properties until the three-dimensional structure of the *Vitis vinifera* enzyme complexed with $NADP^+$ and its natural substrate dihydroquercetin (DHQ) was described. In the course of the study of substrate specificity, crystals of DFR–$NADP^+$–flavonol (myricetin and quercetin) complexes were obtained. Their structures exhibit major changes with respect to that of the abortive DFR–$NADP^+$–DHQ complex. Two flavonol molecules bind to the catalytic site in a stacking arrangement and alter its geometry, which becomes incompatible with enzymatic activity. The X-ray structures of both DFR–$NADP^+$–myricetin and DFR–$NADP^+$–quercetin are reported together with preliminary spectroscopic data. The results suggest that flavonols could be inhibitors of the activity of DFR towards dihydroflavonols.

1. Introduction

Flavonoids constitute a large group of phenolic secondary plant metabolites to which much interest has been devoted owing to their fascinating properties. They play important roles in many plant functions (such as pigmentation, growth and protection against pathogens; Iwashina, 2003; Harbone & Williams, 2000) and exhibit antioxidant activities; they may serve as potential anticancer, anti-arteriosclerosis or anti-inflammatory compounds in human health (Ross & Kasum, 2002; Halliwell *et al.*, 2005; Li *et al.*, 2007; Hertog *et al.*, 1995).

Flavonoids are divided into several classes of compounds which are biogenetically and structurally related. All the compounds share a common C_{15} (C_6-C_3-C_6) structure characterized by a phenylbenzopyran functionality. Each class differs from the others in the degree of oxidation and saturation present in the central heterocyclic *C* ring.

The biosynthetic pathway of these compounds has been widely studied and most of the enzymes that control each single step have been identified from a molecular and biochemical point of view. Several three-dimensional structures of these enzymes have already been described. Among these are the structures of chalcone synthase (CHS; EC 2.3.1.74;

PDB codes 1bi5 and 1cgk; Ferrer *et al.*, 1999), chalcone isomerase (CHI; EC 5.5.1.6; PDB code 1eyp; Jez *et al.*, 2000), anthocyanidin synthase or leucoanthocyanidin dioxygenase (ANS or LDOX; EC 1.14.11.19; PDB code 1gp5; Wilmouth *et al.*, 2002) and 3-*O*-glucosyltransferase (UFGT; EC 2.4.1.91; PDB codes 2c1x, 2c1z and 2c9z; Offen *et al.*, 2006). Recently, we described the first structure of a dihydroflavonol 4-reductase (DFR; EC 1.1.1.219; PDB code 2c29; Petit *et al.*, 2007) at a resolution of 1.8 Å.

DFR is a pivotal enzyme in the flavonoid biosynthesis pathway as it catalyses the last common step (Fig. 1) leading to anthocyanins and proanthocyanidins, two major classes of flavonoids. It catalyses the NADPH-dependent reduction of dihydroflavonols to flavan-3,4-diols. *Vitis vinifera* DFR has been heterologously expressed in *Escherichia coli* and cocrystallized in the presence of one of its natural substrates, dihydroquercetin (DHQ; 3,5,7,3′,4′-pentahydroxyflavanone) and the $NADP^+$ coproduct (this complex is referred to below as complex I). The three-dimensional structure of this complex has been solved and the active-site geometry has been described. Analysis of the interactions between the coproduct, the substrate and the surrounding atoms of the enzyme provides insight into the mechanisms involved in the reduction process. The structure confirms the importance of a segment lining the substrate-binding site and sheds light on the role of residue 133 (Asn or Asp depending on the considered DFR orthologue sequence) previously assumed to control substrate recognition.

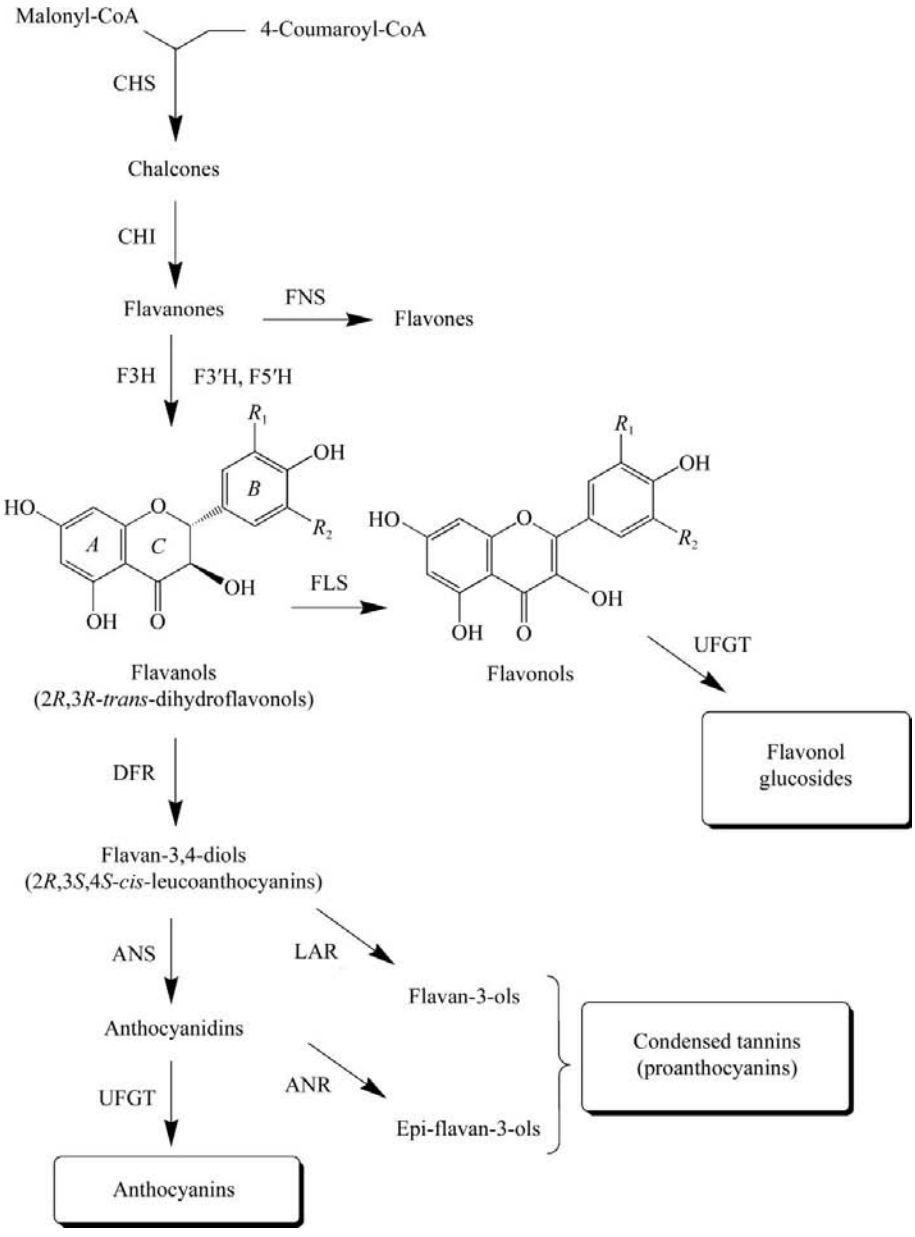

Figure 1
Synthesis pathway of flavonoids. ANR, anthocyanidin reductase; ANS, anthocyanidin synthase (also known as leucoanthocyanidin dioxygenase); CHI, chalcone isomerase; CHS, chalcone synthase; DFR, dihydroflavonol 4-reductase; F3H, flavanone 3-hydroxylase; FLS, flavonol synthase; FNS, flavone synthase; F3′H and F5′H, flavonoid 3′-hydroxylase and 3′,5′-hydroxylase; LAR, leucoanthocyanidin reductase; UFGTs, glucosyl transferases.

In order to shed light on the driving forces of substrate recognition, the structures of different ternary complexes are under active investigation either by mutations in the active site or by complexing the native enzyme with different substrate analogues. In the present study, we describe the complexation properties of DFR with flavonols, one of the most common flavonoid classes present in flowers and fruits, where they act as UV protectants (Flint *et al.*, 1985) and co-pigments (Asen *et al.*, 1972; Scheffeldt & Hrazdina, 1978). We chose flavonols as potential ligands for DFR for several reasons. First of all, flavonols are present in berry fruits throughout their development from flowering to ripening (Jaakola *et al.*, 2002; Downey *et al.*, 2003) and the concentration of quercetin (QUE; 3,5,7,3′,4′-pentahydroxyflavone), one of the major flavonol aglycones, increases in the berry skin of *V. vinifera* cv. Cabernet Sauvignon from veraison to harvest (Fujita *et al.*, 2006). Flavonols are thus present when DFR gene expression occurs, mainly at the veraison and post-veraison stages (Jaakola *et al.*, 2002; Almeida *et al.*, 2007). On the other hand, quercetin has been shown to be an inhibitor of several enzymes, among which is the flavonoid enzyme anthocyanidin reductase from *Medicago truncatula* and *Arabidopsis thaliana* (Xie *et al.*, 2004). Moreover, flavonols and dihydroflavonols present a very similar three-dimensional geometry: whereas the fused rings *A* and *C*

Table 1
X-ray data-collection and refinement statistics.

Values in parentheses are for the last resolution shell.

	Complex II	Complex III
Data statistics		
Resolution range	89.1–2.25 (2.37–2.25)	30.8–2.9 (3.06–2.9)
Completeness (%)	99.7 (99.8)	100 (100)
R_{merge}† (%)	7.9 (28.9)	15.3 (42.5)
Redundancy	3.5 (3.5)	14.3 (14.2)
$I/\sigma(I)$	5.4 (2.0)	4.1 (2.0)
Refinement statistics		
Resolution range	89.1–2.25 (2.31–2.25)	30.8–2.9 (3.06–2.9)
Reflections used for refinement	65910 (4828)	55700 (3729)
Reflections used for R_{free}	3485 (250)	2967 (197)
R_{work}‡	0.186 (0.270)	0.287 (0.282)
R_{free}§	0.255 (0.348)	0.366 (0.460)
No. of protein atoms/average B factor (Å^2)	9981/44.5	15182/26.2
No. of ligand atoms/average B factor (Å^2)	376/36.8	486/16.1
No. of water O atoms/average B factor (Å^2)	768/51.3	129/11.2
R.m.s.d. from ideal geometry		
Bond distances (Å)	0.014	0.013
Bond angles (°)	1.93	2.3
Ramachandran plot		
Most favoured φ/ψ regions (°)	90.8	84.3
Additional allowed φ/ψ regions (°)	8.7	14.4
Disallowed φ/ψ regions (°)	0.0	0.0
Estimated coordinate error (Å)	0.21	0.45

† $R_{merge} = \sum_{hkl}\sum_i |I_i(hkl) - \langle I(hkl)\rangle| / \sum_{hkl}\sum_i I_i(hkl)$, where $\langle I(hkl)\rangle$ is the mean intensity of a set of equivalent reflections. ‡ $R_{work} = \sum\sum |F_{obs} - F_{calc}|/F_{obs}$ for the 95% of the reflection data used in the refinement. F_{obs} and F_{calc} are observed and calculated structure-factor amplitudes, respectively. § R_{free} is the equivalent of R_{work}, except that it was calculated for a randomly chosen 5% test set excluded from refinement.

are rigorously planar in flavonols (Rossi *et al.*, 1986), those of dihydroflavonols exhibit only a slight distortion with a half-chair configuration of ring *C* and a maximum deviation of atoms with respect to the average plane of less than 0.57 Å (Wilmouth *et al.*, 2002; Petit *et al.*, 2007; Selivanova *et al.*, 1999; Xu *et al.*, 2007). Finally, in comparison with dihydroflavonols, flavonols present a higher degree of unsaturation of ring *C*, which modifies the electrophilic and nucleophilic character of the carbonyl in position 4, preventing hydride transfer from the nicotinamide ring of NADPH. This suggests that flavonols could be DFR inhibitors.

In the following, we present the structures of the ternary complexes formed by DFR and NADP$^+$ with two different flavonols, myricetin (MYC; 3,5,7,3′,4′,5′-hexahydroxyflavone) and quercetin (QUE). These structures exhibit strong differences from that of the abortive complex I: two flavonol molecules bind to the active site and disorganize the spatial geometry of the catalytic triad.

Along with these results, we performed preliminary spectroscopic experiments in relation to the activity of DFR in the presence of DHQ and QUE or MYC. Together, these results suggest that flavonols may be inhibitors of DFR activity.

2. Materials and methods

2.1. Enzyme assay

The enzyme activity towards dihydroflavonols was measured in the presence of flavonols following a previously described experimental protocol (Stafford & Lester, 1982; Dédaldéchamp & Uhel, 1999). The assay mixture consisted of 50 m*M* bis-Tris, 50 m*M* tricine pH 6.5, 50 m*M* NaCl, 5 m*M* DTT, to which 1 m*M* NADPH, 1 m*M* DHQ (Fluka, Sigma–Aldrich) and a variable concentration (from 1 to 20 m*M*) of flavonols (QUE from Riedel de Haen or MYC from Fluka) were added (Petit *et al.*, 2007). The reaction was initiated by the addition of 1 µ*M* enzyme and was terminated after 30 min at 303 K by extraction with ethyl acetate (twice). Because leucoanthocyanidin is unstable in solution, the residue was dissolved after evaporation in 1 ml of a mixture of *n*-BuOH and HCl [95:5(*v*:*v*)] and incubated at 368 K for 30 min to form cyanidin. The enzyme activity was estimated from the absorbance at 550 nm arising from cyanidin production.

The steady-state kinetics of DFR were studied as follow. Enzyme assays were carried out at 303 K in 50 m*M* bis-Tris, 50 m*M* tricine, 50 m*M* NaCl, 1%(*v*/*v*) ethanol pH 6.5. Initial rates were estimated from the decrease in absorbance at 340 nm arising from the consumption of both NADPH and DHQ, the molar extinction coefficients of which were 6.22 and 5.15 M^{-1} cm^{-1}, respectively, at pH 6.5. The reaction medium contained 62.5 n*M* DFR and 200 µ*M* initial NADPH. The enzyme was always pre-incubated with NADPH. When used, quercetin was added immediately before the addition of DHQ that initiated the reaction.

2.2. Crystallization and data collection

Crystallization was performed at room temperature (293 K) by hanging-drop vapour diffusion. Drops were prepared on siliconized cover slides and equilibrated against 0.5 or 1.0 ml reservoir solution. The volume of the drops was 4 µl in total, with equal volumes of protein and reservoir solutions. The conditions that led to crystals of DFR complexed with DHQ and NADP$^+$ (Petit *et al.*, 2007) were slightly modified in order to obtain crystals with either MYC or QUE. For both flavonols, the stoichiometry was five equivalents, as for NADP$^+$. The protein concentration was 15 mg ml^{-1} in 10 m*M* tricine, 50 m*M* NaCl, 5 m*M* DTT, 3 m*M* NaN_3 adjusted to pH 7.3.

DFR–NADP$^+$–MYC (complex II) crystals appeared using a reservoir containing 50 m*M* NaCl, 29% PEG 3350, 100 m*M* HEPES pH 6.9 within two weeks and grew to their final size within four weeks. The largest crystals measured 80 × 50 × 50 µm and were cryoprotected with reservoir solution supplemented with 33% glycerol prior to data collection.

DFR–NADP$^+$–QUE (complex III) crystals appeared using a reservoir containing 130 m*M* NaCl, 35% PEG 3350, 100 m*M*

HEPES pH 6.9 within two weeks and grew to their final size within four weeks. The largest crystals measured 260 × 50 × 50 µm and were directly frozen in cold nitrogen gas without any further cryoprotection.

Data collections for DFR-NADP$^+$–MYC and DFR-NADP$^+$–QUE were performed at 100 K using synchrotron radiation on beamlines ID29 and ID14-2, respectively, at the ESRF facility. The data from complex II were indexed in space group $P2_1$ (unit-cell parameters a = 47.23, b = 177.96, c = 92.60 Å, β = 104.8°); those from complex III were indexed in space group $P6_122$ (unit-cell parameters $a = b$ = 174.94, c = 290.18 Å). Data were processed with the program *MOSFLM* (Leslie, 1992) and scaled with the program *SCALA* (Evans, 1997) from the *CCP*4 suite (Collaborative Computational Project, Number 4, 1994). Data-collection statistics are given in Table 1.

2.3. Crystal structure determination

2.3.1. Complex II. Considering the unit-cell size, the asymmetric unit of complex II was expected to be composed of four DFR molecules, which yielded a Matthews coefficient of 2.4 Å^3 Da^{-1} and a solvent content of 47%. The structure was solved by molecular replacement with the program *MOLREP* (Vagin & Teplyakov, 1997) starting from the coordinates of the DFR protein (PDB code 2c29). Using a data resolution cutoff of 3.0 Å, the solution yielded a reliability factor of 0.41 and a correlation coefficient of 0.59.

Early inspection of the electron-density maps showed that several portions of the polypeptide chains (residues 87–92 and 150–169) had drastically moved and needed to be rebuilt. ($mF_o - DF_c$) electron-density maps revealed the presence of the coproduct NADP$^+$ and two flavonol molecules in the vicinity of the catalytic site. The DFR model was modified using the graphics program *Coot* (Emsley & Cowtan, 2004); refinement including NCS restraints was performed with the program *REFMAC* (Murshudov *et al.*, 1997) and controlled throughout with the programs *PROCHECK* (Laskowski *et al.*, 1993), *SFCHECK* (Vaguine *et al.*, 1999) and *WHAT IF* (Vriend & Sander, 1993). Protein stereochemical parameters were taken from Engh & Huber (1991). Heterocompound (NADP$^+$ and MYC) coordinates were taken from the HIC-Up server (Kleywegt & Jones, 1998). Water molecules were positioned in well defined positive ($mF_o - DF_c$) residual densities with a lower cutoff of 3σ if they participated in hydrogen bonds to the protein, ligands or other water molecules. The final model consists of residues 6–88 and 93–329 for chain *A*, residues 1–88 and 92–329 for chain *B*, residues 6–330 for chain *C*, residues 6–88 and 92–329 for chain *D*, one molecule of NADP$^+$ and two molecules of myricetin per chain and a total of 768 water molecules. The six first residues of chain *B* were clearly visible, which is most likely thanks to their singular interaction with a neighbouring molecule in the crystal packing. Superimposition of chains onto one another yielded a 0.30 Å average r.m.s. deviation on C$^\alpha$-atom positions. Final statistics are shown in Table 1.

2.3.2. Complex III. Diffraction data were indexed in a large hexagonal unit cell with parameters $a = b$ = 174.94, c = 290.18 Å. The unit-cell size implied the presence of six molecules in the asymmetric unit, with a Matthews coefficient of 2.7 Å^3 Da^{-1} and a solvent content of 55%. Analysis of the Patterson function results showed a very high peak (45% of the origin-peak value when using data to 8.0 Å resolution) located at (u = 0.333, v = 0.666, w = 0.000), indicating the presence of a pseudo-translation vector. Molecular replacement failed to find the six subunit positions in this large unit cell. Following the method presented by Navaza *et al.* (1998), a molecular-replacement solution was searched for in a smaller unit cell with parameters $a' = b'$ = 101.0, c' = 290.2 Å, γ' = 120°, consistent with the above pseudo-translation vector. Consequently, one third of the collected reflections were used and re-indexed ($h' = h/3 - k/3$, $k' = h/3 + 2k/3$ and $l' = l$), while the space group $P6_122$ was conserved. The volume of the new cell is only one third of the real one and contains only two independent molecules in the asymmetric unit.

Using a monomer of DFR as the search model, the two molecules were successfully positioned using *MOLREP* (R_{fac} = 0.69 for a correlation factor equal to 0.30). The dimeric solution was then used as a search model in the large unit cell and the six independent molecules were unambiguously positioned (R_{fac} = 0.53 for a correlation coefficient equal to 0.58).

The structure reveals the same features as observed for complex II, *i.e.* a displacement

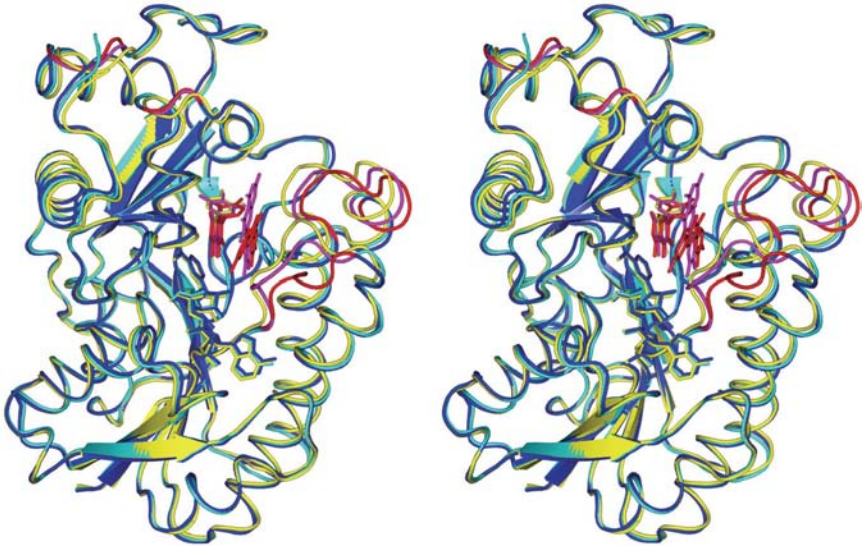

Figure 2
Stereoview of the superimposition of the ternary complexes II (DFR–NADP$^+$–MYC, cyan), III (DFR–NADP$^+$–QUE, blue) onto complex I (DFR–NADP$^+$–DHQ, yellow). DHQ is coloured yellow, MYC pink and QUE red, whereas coproduct NADP$^+$ molecules are coloured yellow (complex I), cyan (complex II) and blue (complex III). Parts of the protein chains that have moved away from structure of complex I are coloured pink and red, respectively.

Table 2
Interactions between the ligand at site *A*, NADP$^+$ and the protein catalytic residues.

Values in parentheses are the estimated standard deviations of the last digits.

	Complex I	Complex II	Complex III
Ligand–protein			
O_4—O^{γ} (Ser128) (Å)	2.85 (3)	3.60 (6)	3.54 (30)
O_3—O^{γ} (Ser128) (Å)	3.24 (4)	2.69 (5)	2.65 (20)
O_4—O^{η} (Tyr163) (Å)	2.62 (8)		
$O_{3'}$—$O^{\delta1}$ (Asn133) (Å)	2.54 (2)	2.62 (6)	2.61 (11)
$O_{4'}$—$N^{\delta1}$ (Asn133) (Å)	3.01 (2)	3.18 (7)	3.07 (15)
$O_{4'}$—$O^{\varepsilon1}$ (Gln227) (Å)	2.54 (1)	2.61 (5)	2.65 (20)
$O_{5'}$—$O^{\varepsilon1}$ (Gln227) (Å)			2.66 (8)
Ligand–NADP$^+$			
C_4—C_4 (Å)	2.94 (8)	3.28 (5)	3.34 (4)
C_4—C_4—N_1 (°)	108.7 (2.8)	88.8 (1.5)	88.6 (3.9)
NADP$^+$–protein			
$O_{2'}$—N^{ζ} (Lys167) (Å)	3.03 (7)	3.41 (7)	3.45 (60)
$O_{3'}$—N^{ζ} (Lys167) (Å)	2.79 (2)	2.87 (6)	2.83 (20)

of loops 86–96 and 150–167 and the presence of two flavonol molecules in the vicinity of the catalytic site. Refinement was carried out as for complex II and the model coordinates of QUE were taken from the HIC-Up server (Kleywegt & Jones, 1998). The final model consists of residues 6–91 and 93–329 for chains *A*, *B*, *C*, *D* and *E* and residues 6–216 and 218–329 for chain *F*, one molecule of NADP$^+$ per chain, nine molecules of quercetin and 135 water molecules. From the shape of the residual electron-density maps ($mF_o - DF_c$), it was only possible to position one quercetin molecule in chain *A* and none in chain *E* because of electron densities that were not well defined. Superimposition of chains onto one another yielded an average r.m.s. deviation on C^{α}-atom positions of 0.30 Å. Final statistics are shown in Table 1.

Atomic coordinates have been deposited in the Protein Data Bank with accession codes 3c1t and 3bxx. The figures were drawn using *PyMOL* (DeLano, 2002).

3. Results

A comparison between the structures of complexes II and III and that of complex I is illustrated in Fig. 2, in which the structures have been superimposed onto complex I as a reference: the most striking difference is the presence of two flavonols observed in the vicinity of the catalytic site. The presence of the flavonols is responsible for the drastic displacement of the loops that wrap up the flavonol molecules, *i.e.* regions 87–96 and 150–169; the largest C^{α} r.m.s. deviations from complex I (see Fig. 3) are observed for these loops and are 0.643 and 0.994 Å overall when superimposing complex II and complex III onto complex I, respectively. Figs. 4(*a*) and 4(*b*) illustrate the quality of the ($2mF_o - DF_c$) electron-density map for both the coproduct and flavonol molecules in complexes II and III, respectively.

3.1. NADP$^+$-binding site

The presence of two flavonol molecules has no major consequences on the geometry and binding of the coproduct (see Fig. 4*c*). The protein–NADP$^+$ hydrogen bonds and van der Waals contacts do not vary in a significant manner. One contact to the catalytic triad residues, Tyr163 O^{η}–$O^{2'}$, is absent because of the presence of the second flavonol molecule nearby (see below).

3.2. Flavonol-binding site *A*

In the structures of both complexes II and III, one of the two flavonol molecules (MYC*A* or QUE*A*) binds to the protein at the DHQ-binding site as observed in complex I (Figs. 4*c* and 5*b*) and exhibits a conformation that differs from that of DHQ, mostly because its fused *A*–*C* rings adopt a planar conformation. On the other hand, the dihedral-angle (O_1—C_2—$C_{1'}$—$C_{2'}$) values which account for the rotation of ring *B* relative to the fused *A*–*C* rings are very similar: 113.7, 108.7 and 109.7° for complexes I, II and III, respectively.

Each of the MYC*A* and QUE*A* molecules is slightly translated (about 0.6 Å) with respect to the DHQ position (Figs. 4*c* and 5*b*) along a direction parallel to the C_2—$C_{1'}$ axis. As a consequence, the distances between the flavonol, the coproduct and two of the catalytic residues, Ser128 and Lys167, are noticeably modified from those observed in complex I (Table 2), in particular Ser128 O^{γ}—O_4 (MYC*A* or QUE*A*), Lys167 N^{ζ}—$O_{2'}$ (NADP$^+$) and C_4 (MYC*A* or QUE*A*)—C_4 (NADP$^+$).

Finally, the contacts between the hydroxyl groups of ring *B* and the side chains of residues Asn133 and Gln227 are conserved for both flavonols in site *A*. In both structures, the flavonol molecule appears to be almost fully embedded within the protein: the fraction of its surface area which remains accessible to solvent is only 1% and 3% of its total surface area for MYC*A* and QUE*A*, respectively.

3.3. Flavonol-binding site *B*

A second flavonol molecule binds the protein near site *A* (Figs. 5*a* and 5*b*). The molecules are almost planar; the dihedral angles (O_1—C_2—$C_{1'}$—$C_{2'}$) are −3.9 and −21.8° for MYC*B* and QUE*B*, respectively. Both stack onto the fused ring *A*–*C* of molecule *A* with a maximum overlap with rings *B* and *C*. Inter-planar contacts between molecules *A* and *B* range from 3.0 to 3.7 Å.

However, molecules MYC and QUE do not bind to site *B* in the same manner (Fig. 5*b*). With respect to QUE*B*, the MYC*B*

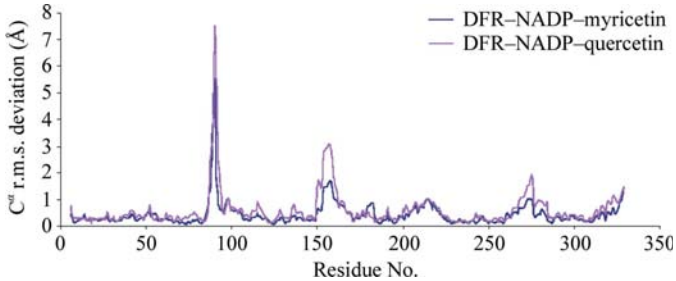

Figure 3
Plot of the C^{α} r.m.s. deviations (Å) between complex II and complex I (blue) and between complex III and complex I (purple).

molecule is rotated by almost 180° around a direction close to that defined by $C_2-O_{4'}$. In principle, a molecule of QUE could adopt the orientation observed for MYC, but the reverse does not seem to be possible because of steric hindrance of the third hydroxyl group of the MYC *B* ring, which would clash with the phenyl ring of residue Phe160. The two ring *B* hydroxyl groups common to MYC*B* and QUE*B* interact with that of residue Ser128, whereas the third hydroxyl group of MYC*B* is hydrogen bonded to $O_{2'}$ of the nicotinamide sugar. Finally, for both MYC*B* and QUE*B* molecules, all the hydroxyl groups of the fused rings *A*–*C* are exposed to the solvent and hydrogen bonded to water molecules. At site *B*, the molecules appear to be slightly more exposed to solvent than molecules in site *A*. Their accessible surface areas are 9% and 18% of the total surface area for MYC*B* and QUE*B*, respectively.

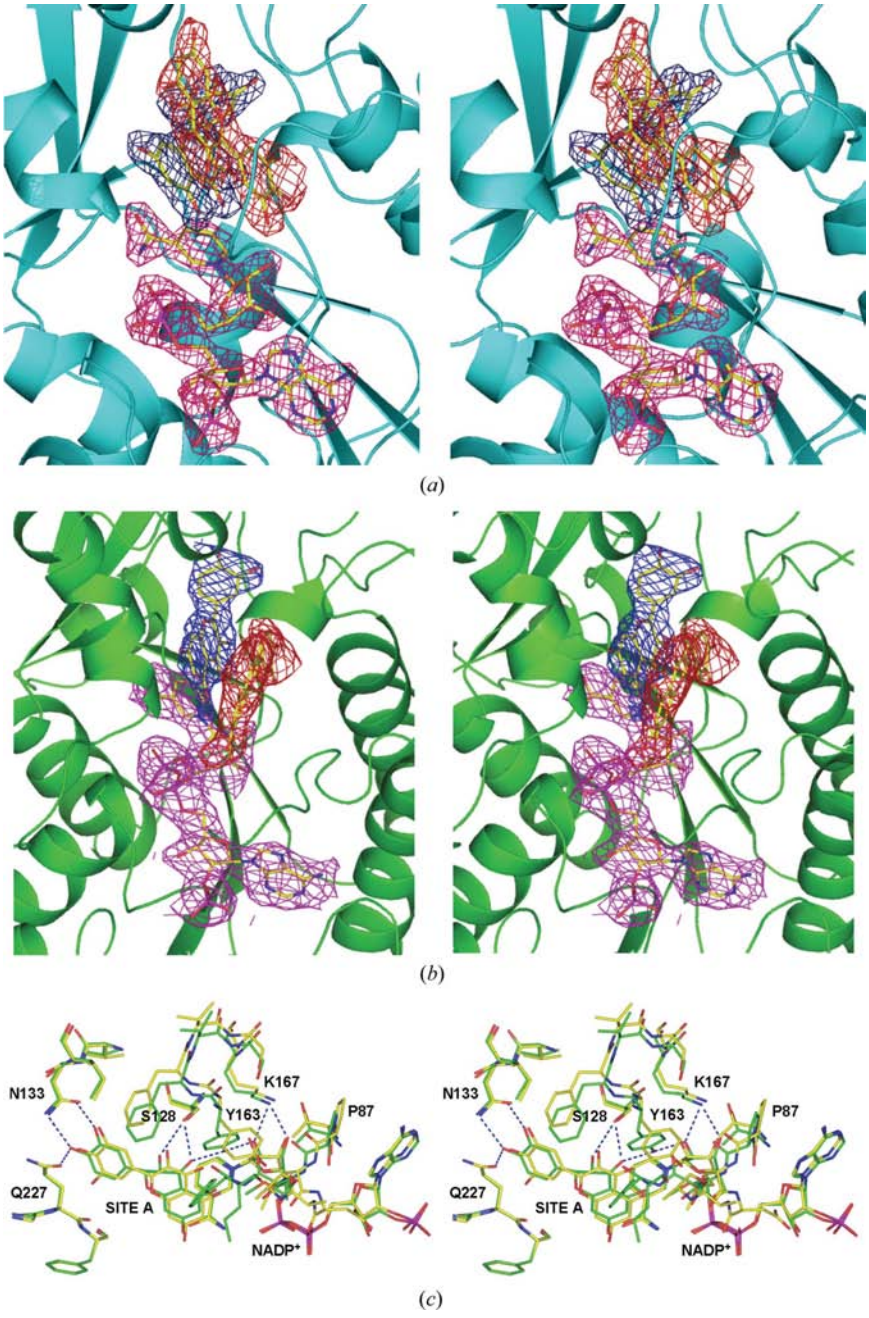

Figure 4
(*a*) Stereoview of NADP$^+$ and two molecules of myricetin bound to DFR. The ($2mF_o - DF_c$) electron-density map is contoured at the 2 r.m.s. level. Pink, blue and red densities are for NADP$^+$, MYCA and MYCB, respectively. (*b*) Stereoview of NADP$^+$ and two molecules of quercetin bound to DFR. The ($2mF_o - DF_c$) electron-density map is the NCS map average contoured at the 2 r.m.s. level. (*c*) Stereoview of a superimposition of complexes I and II at the myricetin-binding site *A*. Myricetin binding at site *B* has been omitted for clarity. The C atoms of complex I are coloured green; those of complex II are coloured yellow. Interactions between protein atoms of the catalytic site and the coproducts refer to the structure of complex I.

4. Discussion

The planar conformation of the fused rings *A* and *C* is responsible for the tight interactions between the two flavonol molecules. It is noteworthy that the inter-planar contacts (3.0–3.7 Å) are the same as those found in the molecular crystal packing of quercetin (Rossi *et al.*, 1986) or quercetin dihydrate (Jin *et al.*, 1990), for which the unit-cell parameters corresponding to the stacking direction are 3.725 and 3.719 Å, respectively.

Similar binding at the active site of an enzyme has previously been encountered in the double mutant W219Y/C298A of human aldose reductase (Harrison *et al.*, 1997). Two molecules of alrestatin, a planar inhibitor of aldose reductase, bind the enzyme mutant in a stacked arrangement. Interestingly, the accommodation of such a bulky entity in the active site led to a change in the orientation of an aromatic side-chain amino acid, Trp20, in order to undergo stacking interactions with one of the two inhibitor molecules.

In DFR, the consequences of the stacking of two flavonol molecules are even more dramatic. It leads to the rotation of the side chain of one of the catalytic residues, Tyr163, which turns away from the catalytic site. This residue now appears in an inactive form: it is no longer able to play the role of a catalytic base by providing the oxygen of the carbonyl group C_4O_4 of the site *A* ligand with a proton. The new orientation of Tyr163 favours stacking interactions of its aromatic ring with that of molecule *B* in the present structure. This type of interaction, previously observed in the aldose reductase mutant, seems to be relevant to the binding process of two flavonol molecules to the enzyme. It is illustrated in Fig. 6, in which the stacking of successive saturated and aromatic rings is highlighted between residue Pro190, the nicotinamide ring, molecules *A* and *B* and residue Tyr163.

The above-described structures, compared with that of complex I, demonstrate that DFR from grapes can host either flavonols or dihydroflavonols, since both MYC*A* and QUE*A* molecules can bind to the active site in a similar way to DHQ. Rather limited differences in the steric hindrance of the two molecules may account for this competitive binding mode. The deviation from planarity of the fused rings *A* and *C* of DHQ remains limited (the highest deviation from the mean plane is 0.56 Å; Selivanova *et al.*, 1999) and the *B* phenyl ring can adopt different orientations relative to the heterocyclic system, so that the active site is able to accommodate each molecule without drastic structural changes.

The change in the orientation of Tyr163 can only be explained by steric hindrance arising from the presence of the second flavonol molecule stacked against the first one in the active site. Thus, the stacking arrangement of the two flavonol molecules is most likely to be the driving force that leads to the inactive state of the enzyme.

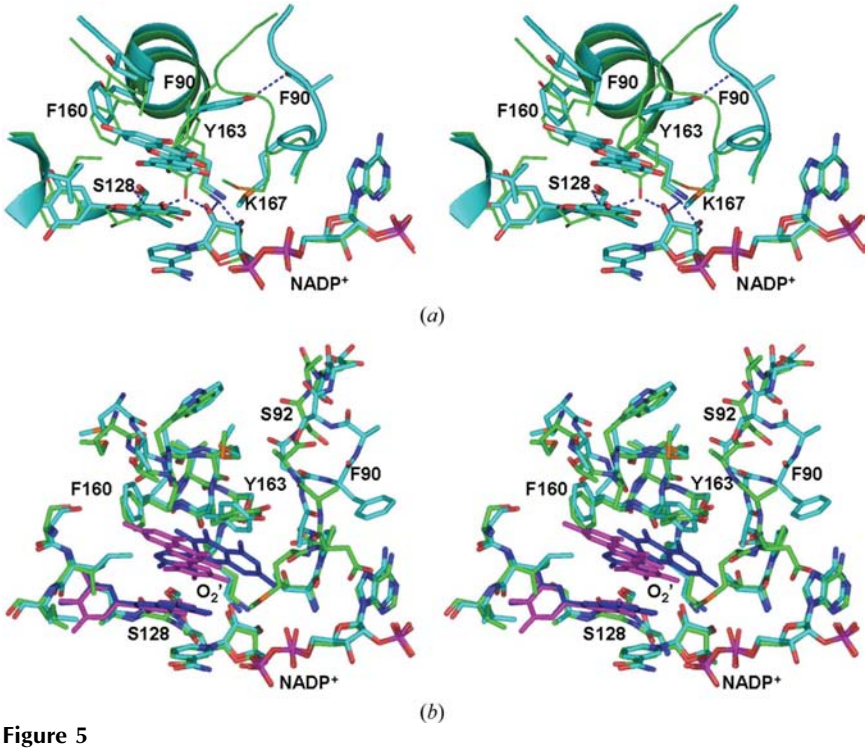

Figure 5
(*a*) Stereoview of a superimposition of complexes I and II in the vicinity of the catalytic site. The C atoms of complexes I and II are shown in green and cyan, respectively. (*b*) Stereoview of a superimposition of complexes II and III in the vicinity of the catalytic site. The C atoms of complexes II and III are shown in cyan and green, respectively. Molecules of myricetin and quercetin are shown in purple and dark blue, respectively.

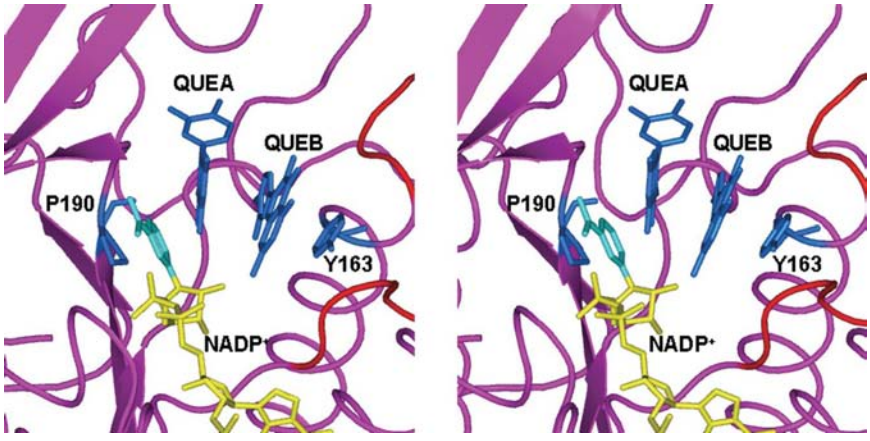

Figure 6
Stereoview illustrating the stacking of saturated and aromatic rings of protein, flavonols and NADP$^+$ in the vicinity of the catalytic site of complex III.

These structural results do not allow us to discuss the influence of a change in the *C*-ring charge delocalization between dihydroflavonols and flavonols on the DFR activity since we have so far failed to obtain crystals with only one flavonol molecule in the active site. However, they clearly demonstrate that DFR is not specific for dihydroflavonols. Moreover, this enzyme exhibits high flexibility since it may accommodate two molecules in the active site.

To further investigate the behaviour of DFR in the presence of flavonols, the enzyme activity was assayed by measuring the remaining cyanidin-production activity of DFR in the presence of various amounts of flavonols. Cyanidin production continuously decreased (Fig. 7*a*) as a function of flavonol concentration. These preliminary spectroscopic results reinforce the structural results and suggest possible inhibition of the reaction by flavonols. Nevertheless, they are based on cyanidin production, which was only measured long after the reaction was completed. Kinetic studies investigating NADPH consumption at 340 nm are currently under investigation. Initial results obtained with quercetin confirm the inhibition.

Control experiments performed in the absence of DHQ confirmed that DFR did not possess quercetin reductase activity.

Using DHQ as a substrate, the initial rates of DFR were markedly decreased at much lower concentrations of quercetin than those used in crystallization or activity experiments. No pre-steady-state lag time was observed, which means that quercetin is a fast and reversible inhibitor.

As shown in Fig. 7(*b*), Lineweaver–Burk plots of $1/V$ as a function of 1/[DHQ] give straight lines intersecting the $1/V$ axis, demonstrating that quercetin acts as a simple competitive inhibitor with mutually exclusive binding of DHQ and quercetin. In the presence of quercetin, $K_{M(DHQ)}$ is therefore increased by a factor $\{1 + [QUE]/K_{i(QUE)}\}$. The inhibition constant $K_{i(QUE)}$ is

the dissociation constant of the ternary complex *E*–NADPH–QUE, since NADPH is the first substrate that adds to the enzyme in a sequential ordered mechanism (Trabelsi *et al.*, in preparation).

Based on these data, the average estimation of $K_{i(QUE)}$ is 3.8 μM, a value that is sufficiently low to suggest that inhibition of DFR by quercetin may be physiologically relevant. Unfortunately, high concentrations of quercetin could not be used owing to its rather high rate of oxidative degradation. Therefore, no evidence of parabolic inhibition could be found and our kinetic data cannot be used to determine the range of quercetin concentrations under which a quaternary complex containing two equivalents of quercetin builds up. However, they do suggest that the quaternary complex *E*–NADPH–$(QUE)_2$ that has been crystallized is derived from the ternary complex *E*–NADPH–QUE.

The relevance of these results has to be discussed from a physiological point of view. It is now well known that both flavonols and dihydroflavonols are synthesized in the same cellular compartment, the cytosol, before being transported to the vacuole (van Eldik *et al.*, 1997; Gould *et al.*, 2002). Moreover, flavonol biosynthesis is observed throughout berry development; the greatest increase in flavonols in the berry is observed three to four weeks post-veraison (Downey *et al.*, 2003), *i.e.* when DFR is expressed (Boss *et al.*, 1996).

Thus, it could be possible that FLS competes with DFR, since both enzymes transform the same substrate and since flavonols, the products of FLS, can bind to the active site of DFR. However, flavonoid-biosynthesis enzymes are believed to form multi-enzyme complexes associated with the cytoplasmic face of the endoplasmic reticulum (Hrazdina & Wagner, 1985; Burbulis *et al.*, 1996), as has been shown for CHS, CHI and DFR (Burbulis & Winkel-Shirley, 1999). If DFR and FLS were part of separate complexes, then their activities could be independent: their respective products would only be the substrates of enzymes belonging to the same complex.

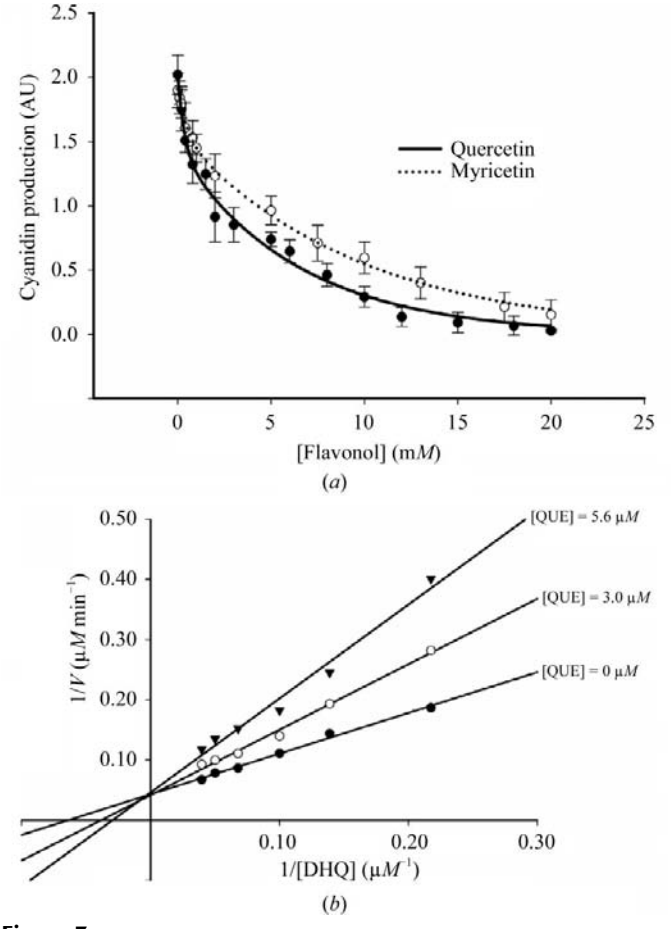

Figure 7
(*a*) Concentration-dependence of cyanidin production from DFR activity as a function of flavonol concentration (1–20 mM) in the presence of DHQ (1 mM). Cyanidin production was measured as optical absorption at 550 nm. Error bars represent ± 1 standard deviation. (*b*) Lineweaver–Burk plots observed for increasing concentrations of quercetin.

We thank the European Synchrotron Radiation Facility (Grenoble, France) for provision of synchrotron-radiation facilities and the staff of the ID29 and ID14-2 beamlines for their kind assistance. We also thank Professor Serge Delrot (Institut de la Vigne et du Vin, Villenave d'Ornon, France) for critical reading of the manuscript. This work was supported by the CIVB (Conseil Interprofessionnel du Vin de Bordeaux).

References

Almeida, J. R. M., D'Amico, E., Preuss, A., Carbone, F., Ric de Vos, C. H., Deiml, B., Mourgues, F., Perrotta, G., Fischer, T. C., Bovy, A. G., Martens, S. & Rosati, C. (2007). *Arch. Biochem. Biophys.* **465**, 61–71.
Asen, S., Stewart, R. N. & Norris, K. H. (1972). *Phytochemistry*, **11**, 1139–1144.
Boss, P. K., Davies, C. & Robinson, S. P. (1996). *Plant Physiol.* **111**, 1059–1066.
Burbulis, I. E., Pelletier, L. K., Cain, C. C. & Shirley, B. W. (1996). *SAAS Bull. Biochem. Biotechnol.* **9**, 29–36.
Burbulis, I. E. & Winkel-Shirley, B. (1999). *Proc. Natl Acad. Sci. USA*, **96**, 12929–12934.
Collaborative Computational Project, Number 4 (1994). *Acta Cryst.* D**50**, 760–763.
Dédaldéchamp, F. & Uhel, C. (1999). *Enzyme Microb. Technol.* **25**, 316–321.
DeLano, W. L. (2002). *The PyMOL Molecular Graphics System.* http://www.pymol.org.
Downey, M. O., Harvey, J. S. & Robinson, S. P. (2003). *Aust. J. Grape Wine Res.* **9**, 110–121.
Eldik, G. J. van, Reijnen, W. H., Ruiter, R. K., van Herpen, M. M., Schrauwen, J. A. & Wullems, G. J. (1997). *Plant J.* **11**, 105–113.
Emsley, P. & Cowtan, K. (2004). *Acta Cryst.* D**60**, 2126–2132.
Engh, R. A. & Huber, R. (1991). *Acta Cryst.* A**47**, 392–400.
Evans, P. R. (1997). *Jnt CCP4/ESRF–EACBM Newsl. Protein Crystallogr.* **33**, 22–24.
Ferrer, J.-L., Jez, J. M., Bowman, M. E., Dixon, R. A. & Noel, J. P. (1999). *Nature Struct. Biol.* **6**, 775–784.
Flint, S. D., Jordan, P. W. & Caldwell, M. M. (1985). *Photochem. Photobiol.* **41**, 95–99.
Fujita, A., Goto-Yamamoto, N., Aramaki, I. & Hashizume, K. (2006). *Biosci. Biotechnol. Biochem.* **70**, 632–638.
Gould, K. S., McKelvie, J. & Markham, K. R. (2002). *Plant Cell Environ.* **25**, 1261–1269.
Halliwell, B., Rafter, J. & Jenner, A. (2005). *Am. J. Clin. Nutr.* **81**, 268–276.
Harbone, J. B. & Williams, C. A. (2000). *Phytochemistry*, **55**, 481–504.

Harrison, D. H. T., Bohren, K. M., Petsko, G. A., Ringe, D. & Gabbay, K. H. (1997). *Biochemistry*, **36**, 16134–16140.
Hertog, M. G., Kromhout, D., Aravanis, C., Blackburn, H., Buzina, R., Fidanza, F., Giampaoli, S., Jansen, A., Menotti, A. & Nedejikovic, S. (1995). *Arch. Intern. Med.* **155**, 381–386.
Hrazdina, G. & Wagner, G. J. (1985). *Arch. Biochem. Biophys.* **237**, 88–100.
Iwashina, T. (2003). *Biol. Sci. Space*, **17**, 24–44.
Jaakola, L., Määttä, K., Pirttilä, A. M., Törrönen, R., Kärenlampi, S. & Hohtola, A. (2002). *Plant Physiol.* **130**, 729–739.
Jez, J. M., Bowman, M. E., Dixon, R. A. & Noel, J. P. (2000). *Nature Struct. Biol.* **7**, 786–791.
Jin, G.-Z., Yamagata, Y. & Tomita, K. (1990). *Acta Cryst.* C**46**, 310–313.
Kleywegt, G. J. & Jones, T. A. (1998). *Acta Cryst.* D**54**, 1119–1131.
Laskowski, R. A., MacArthur, M. W., Moss, D. S. & Thornton, J. M. (1993). *J. Appl. Cryst.* **26**, 283–291.
Leslie, A. G. W. (1992). *Jnt CCP4/ESF–EACBM Newsl. Protein Crystallogr.* **26**.
Li, Y., Fanq, H. & Xu, W. (2007). *Mini Rev. Med. Chem.* **7**, 663–678.
Murshudov, G. N., Vagin, A. A. & Dodson, E. J. (1997). *Acta Cryst.* D**53**, 240–255.
Navaza, J., Panepucci, E. H. & Martin, C. (1998). *Acta Cryst.* D**54**, 817–821.
Offen, W., Martinez-Fleites, C., Yang, M., Kiat-Lim, E., Davis, B. G., Tarling, C. A., Ford, C. M., Bowles, D. J. & Davies, G. J. (2006). *EMBO J.* **25**, 1396–1405.
Petit, P., Granier, T., Langlois d'Estaintot, B., Manigand, C., Bathany, K., Schmitter, J. M., Lauvergeat, V., Hamdi, S. & Gallois, B. (2007). *J. Mol. Biol.* **368**, 1345–1357.
Ross, J. A. & Kasum, C. M. (2002). *Annu. Rev. Nutr.* **22**, 19–34.
Rossi, M., Rickles, L. F. & Halpin, W. A. (1986). *Bioorg. Chem.* **14**, 55–69.
Scheffeldt, P. & Hrazdina, G. (1978). *J. Food Sci.* **43**, 517–520.
Selivanova, I. A., Tyukavkina, N. A., Kolesnik, Y. A., Nesterov, V. N., Kuleshova, L. N., Khutoryanskii, V. A., Bazhenov, B. N. & Saibotalov, M. Y. (1999). *Pharm. Chem. J.* **33**, 222–224.
Stafford, H. A. & Lester, H. H. (1982). *Plant. Physiol.* **70**, 695–698.
Vagin, A. & Teplyakov, A. (1997). *J. Appl. Cryst.* **30**, 1022–1025.
Vaguine, A. A., Richelle, J. & Wodak, S. J. (1999). *Acta Cryst.* D**55**, 191–205.
Vriend, G. & Sander, C. (1993). *J. Appl. Cryst.* **26**, 47–60.
Wilmouth, R. C., Turnbull, J. J., Welford, R. W., Clifton, I. J., Prescott, A. G. & Schoefield, C. J. (2002). *Structure*, **10**, 93–103.
Xie, D.-Y., Sharma, S. B. & Dixon, R. A. (2004). *Arch. Biochem. Biophys.* **422**, 91–102.
Xu, Z., Liu, B., Ning, Z. & Zhang, Y. (2007). *Acta Cryst.* E**63**, o4384.